Optical Properties of Responsive Hybrid Au@Polymer Nanoparticles

Mario Tagliazucchi,[†] Martin G. Blaber,[†] George C. Schatz,[†] Emily A. Weiss,[†] and Igal Szleifer[†,‡,*]

[†]Department of Chemistry and [‡]Department of Biomedical Engineering and Chemistry of Life Processes Institute, Northwestern University, 2145 Sheridan Road, Evanston, Illinois 60208-3113, United States

ABSTRACT

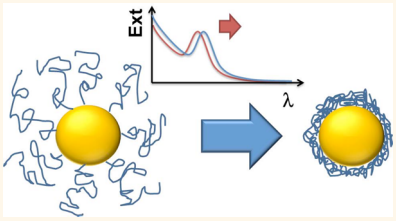

This work presents a novel modeling approach to calculate the optical properties of gold nanoparticles coated with stimuli-responsive polymers. This approach combines, for the first time, a molecular description of the soft material with an electrodynamics calculation of the optical properties of the system. A mean-field molecular theory is first used to calculate the local density of the polymer and the position-dependent dielectric constant surrounding the nanoparticle. This information is then used to calculate the optical properties of the Au@polymer colloid by solving Maxwell's equations for an incident electromagnetic wave. Motivated by the interest in Au@PNIPAM and Au@PVP experimental systems, the theory is applied to study the effect of polymer collapse on the position of the localized surface plasmon resonance (LSPR) of the system. The most important results of the present study are as follows: (i) the LSPR always shifts to lower energies upon polymer collapse (in agreement with experimental results); this observation implies that the red shift expected due to increasing polymer density always overcomes the blue shift expected from decreasing layer thickness; (ii) the magnitude of the LSPR shift depends nonmonotonically on surface coverage and nanoparticle radius; and (iii) the formation of aggregates on the nanoparticle surface (due to microphase segregation) decreases the magnitude of the LSPR shift. These results highlight the importance of explicitly considering the coupling between the soft material and the inorganic components in determining the optical properties of the hybrid system.

KEYWORDS: localized surface plasmon resonance · gold nanoparticle · stimuli-responsive polymer · Mie theory · discrete dipole approximation · molecular theory · LSPR sensing

The synergistic combination of soft and inorganic nanomaterials promises new classes of hybrid systems, in which the stimuli-responsive properties of the soft component[1] modulate the optical, electrical, catalytic, magnetic, and transport properties of the inorganic component. Specific examples in this area are composites of gold and silver nanoparticles (NPs) with polymeric materials for plasmonic nanosensors,[2−4] switchable catalysts[5] and light-reconfigurable materials,[6] polymer-modified nanopores for pH- or temperature-switchable transport,[7−12] and polymeric materials loaded with magnetic nanoparticles exhibiting coupled magnetic and mechanical properties.[13,14] These "smart" materials present a higher degree of physical and chemical complexity than the isolated components. This complexity, which arises because the properties of the components are nonadditive, leads to new function (*e.g.*, the transport properties of polyelectrolyte-modified nanopores cannot be understood from the individual transport properties of the bare nanopores and the polyelectrolyte in the bulk[8,9]). The fundamental understanding of hybrid systems therefore challenges existing models and intuition derived for homogeneous systems and requires new theoretical approaches in order to couple the organization of the soft molecular component with the properties of the inorganic part.

In this paper, we present a new modeling approach to study the optical properties of Au nanoparticles (NPs) coated by polymeric shells. The position of the localized surface plasmon resonance (LSPR) in hybrid Au NP/responsive polymer composites can be tuned by changes in the chemical or physical environment through three mechanisms: (i) coupling/decoupling of plasmons of individual particles due to changes in the interparticle distance as the soft component switches shape (*e.g.*, in polymer-linked NPs or Au-NP-decorated hydrogels[4]); (ii) changes in the density of conduction electrons due to electrochemical charging of the metallic core;[15] and (iii) changes in the local refractive index around the particle due to changes in the density or thickness of the polymeric layer. In this work, we will focus our attention on core−shell Au@polymer colloids[3,16−19] (where the notation Au@polymer describes a polymer-coated gold nanoparticle). In these

* Address correspondence to igalsz@northwestern.edu.

Received for review July 18, 2012 and accepted August 20, 2012.

Published online August 21, 2012
10.1021/nn303221y

systems, the LSPR shift is mainly attributable to mechanism *iii*, more specifically, to changes in the local refractive index produced by polymer collapse (a collapsed polymer film contains no or very little solvent, and thus it is a compact layer, in opposition to swollen polymer films that have a large solvent content). Most experimental work on Au@polymer colloids shows a decrease in the particle hydrodynamic radius (as measured by dynamic light scattering, DLS) upon polymer collapse,[16,18] and therefore, nanoparticle aggregation (which would lead to an increase in particle size) can be ruled out. In those experiments, mechanism *i* (plasmon shift due to plasmon coupling between particles) cannot contribute to the observed shift of the LSPR. A contribution from mechanism *ii*, change in the density of free charge carriers, to the LSPR shift requires transfer of electronic density from/to the gold core, which can occur under electrochemical control, in the presence of redox species or strongly adsorbed polyvalent ions.[20] These conditions, however, are not present in most Au@polymer experiments, so mechanism *ii* can be also ruled out for the systems of interest.

Examples of stimuli-responsive Au@polymer colloids are Au@poly(*N*-isopropylacrylamide) (PNIPAM), which displays a red shift of the LSPR for temperatures above the collapse temperature of PNIPAM[16,18,19,21] and Au@poly(4-vinylpyridine) (PVP) that shows a similar behavior when the solution pH is increased above the collapse pH of PVP.[22] Interestingly, predicting *a priori* the direction of the shift of the LSPR due to polymer collapse in Au@polymer colloids is nontrivial: a collapse of the polymer shell decreases film thickness (this effect alone will promote a blue shift of the LSPR) but also increases the internal polymer density of the film (this effect alone will promote a red shift of the LSPR because the refractive index of PNIPAM and PVP is higher than that of water).

Our approach to model the optical properties of Au@polymer particles consists of (i) determining the structure of the polymer layer using a free-energy functional theory that considers the molecular details of the grafted macromolecules, (ii) using the structure of the polymer layer to calculate the heterogeneous dielectric environment around the particle, and (iii) calculating the optical properties of the system by solving Maxwell's equations for an incident electromagnetic wave interacting with the Au@polymer system, while treating the Au particles explicitly. Motivated by the recent interest in Au@PNIPAM as a thermoswitchable plasmonic system, we use our theory to systematically study the change in the position of the LSPR peak as the soft shell evolves from a swollen to a collapsed state. We show that the collapse of the end-grafted polymer layer resulting from decreasing the effective quality of the solvent always results in a red shift of the LSPR band. The magnitude of the shift nonmonotonically depends on the grafting density (the number of polymers grafted on the surface of the nanoparticle divided by its surface area) and the radius of the Au core. These results highlight the importance of a proper structural description of the soft material component of the hybrid systems in determining the plasmon resonance and provide design rules for stimuli-responsive plasmonic materials.

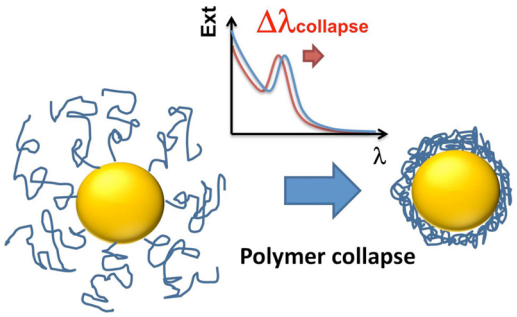

Figure 1. Scheme of the system under study. A gold nanoparticle of radius *R* is coated by an end-grafted polymer layer with a surface density σ and a chain length *N*. The collapse of the grafted polymer layer due to an increase in the effective quality of the solvent (χ) produces a shift $\Delta\lambda_{collapse}$ in the position of the LSPR peak.

RESULTS AND DISCUSSION

Description of the Model System. Figure 1 shows the system under study: a Au NP spherical core of radius *R* and surface area *A* coated with n_p end-grafted polymers of chain length *N* and surface coverage $\sigma = n_p/A$ (number of grafted polymers per unit area). On the basis of the assertion that collapse/swell of the soft matter shell is the main mechanism for LSPR switching in Au@PNIPAM[3,16,18,19,23] and Au@PVP,[22] we will investigate specifically the effect of polymer reorganization on the LSPR. The driving force for the collapse is the change in the quality of the solvent (*i.e.*, change in the solubility of the polymer). The solubility depends on the difference between the polymer−polymer and polymer−water attractive forces (these forces include van der Waals and hydrogen bonding interactions). In order to keep the discussion general, we have chosen to use a single parameter (χ) to model the effective quality of the solvent. The χ parameter controls the strength of the interaction forces between segments; changes in χ, therefore, mimic changes in temperature or pH for PNIPAM or PVP, respectively. This simplified description captures the effect of polymer collapse on the optical properties of the system, regardless of the specific driving force for collapse. Details of the molecular organization of the polymer layer may depend on pH or temperature effects.[24]

Effect of Solvent Quality, Chain Length, and Surface Coverage on the LSPR. Figure 2A shows the polymer volume fraction (fraction of a given three-dimensional space that is occupied by polymer segments) as a function of the radial coordinate for a spherical Au core of $R = 5$ nm, $N = 150$, $\sigma = 0.25$ chains·nm^{-2}, and different values of χ. In this calculation, we assumed radial symmetry; that is,

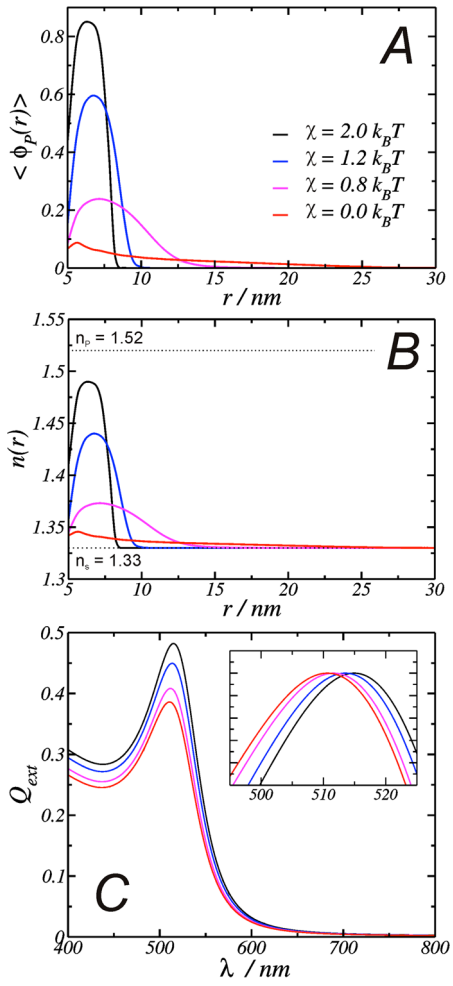

Figure 2. (A) Polymer volume fraction profile as a function of the radial coordinate for a nanoparticle of R = 5 nm, N = 150, σ = 0.25 chains·nm^{-2}, and different values of the quality of the solvent parameter χ. (B) Local refractive index profile as a function of the radial coordinate calculated from the polymer volume fraction profiles in A. The dotted lines show the refractive index of pure polymer (n_p) and pure solvent (n_s). (C) Calculated extinction (absorption + scattering) spectra for the systems in A. The inset shows the normalized extinction spectra.

the film is inhomogeneous only in the radial coordinate. Changing χ from 0 k_BT (good solvent) to 2 k_BT (poor solvent) causes a polymer collapse that produces a decrease in film thickness and an increase in the average polymer volume fraction. Figure 2B shows the r-dependent refractive index, $n(r)$, determined from the polymer volume fraction profiles. Using the r-dependent refractive index, we calculated the extinction spectra for different values of χ (see Figure 2C). For the values of R, N, and σ used in the calculations of Figure 2, polymer collapse is predicted to produce a red shift of 4.3 nm and to increase the extinction coefficient; this increase occurs due to the shift of the LSPR away from interband transitions of gold.

In contrast to inorganic shells, which present a well-defined and homogeneous thickness and refractive index, polymeric shells have a thickness and refractive

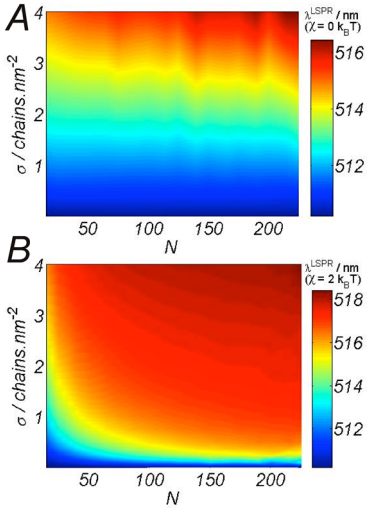

Figure 3. Position of the LSPR as a function of chain length (N) and grafting density (σ) for a Au core of R = 5 nm and χ = 0 k_BT (good solvent, panel A) or χ = 2 k_BT (poor solvent, panel B).

index that depend nontrivially on the molecular structure of the polymer and on environmental conditions. Figure 3A,B shows the predicted position of the LSPR band (λ^{LSPR}) for χ = 0 and 2 k_BT (good and a poor solvents, respectively) for different surface coverages (σ) and chain lengths (N) of the polymer. In good solvent, λ^{LSPR} increases with σ but is rather insensitive to N. Simple scaling arguments[25,26] show that film thickness for a polymer brush in a good solvent increases as $N\cdot\sigma^{1/3}$. The internal volume fraction of the polymer (which controls the refractive index of the film) is proportional to the ratio of number of polymer segments per unit area ($N\cdot\sigma$) to the thickness of the layer ($N\cdot\sigma^{1/3}$), and thus it scales as $\sigma^{2/3}$. Since λ^{LSPR} for χ = 0 is rather insensitive to N but varies with σ, we conclude that the internal volume fraction of the polymer is the main factor controlling the optical properties in a good solvent. In a poor solvent, the internal volume fraction of the polymer is rather constant and very close to 1 (Figure 2A); therefore, in this case, the film thickness controls the position of the LSPR. The thickness of the film in a poor solvent is proportional to the product $N\cdot\sigma$, which explains why λ^{LSPR} depends both on N and σ for a collapsed polymer (χ = 2 k_BT in Figure 3B).

Collapse of the Polymer Always Leads to a Red Shift of the LSPR. An important parameter in experimental studies and potential sensing applications is the shift in the LSPR peak following polymer collapse, that is, the difference between the λ^{LSPR} values shown in Figure 3B and those shown in Figure 3A. We introduce the variable $\Delta\lambda_{collapse}$ as the shift of the LSPR peak wavelength between the collapsed and swollen states:

$$\Delta\lambda_{collapse} = \lambda^{LSPR}(\chi = 2\,k_BT) - \lambda^{LSPR}(\chi = 0\,k_BT) \quad (1)$$

Figure 4A shows a color map of $\Delta\lambda_{collapse}$ as a function of N and σ. An important conclusion from this plot is

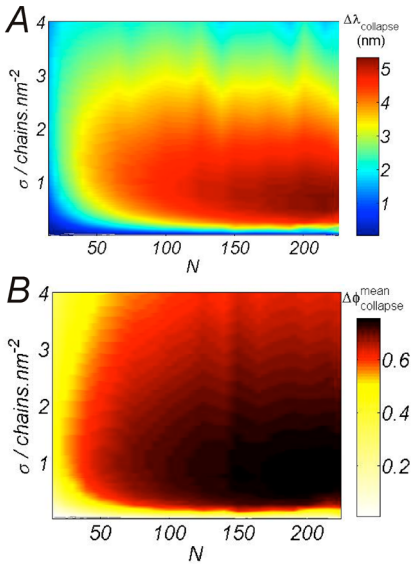

Figure 4. Change in the position of the LSPR band ($\Delta\lambda_{collapse}$, see eq 1, panel A) and the average polymer volume fraction of the film ($\Delta\phi^{mean}_{collapse}$, see eq 2, panel B) upon film collapse, as a function of chain length (N) and grafting density (σ) for a Au core of R = 5 nm.

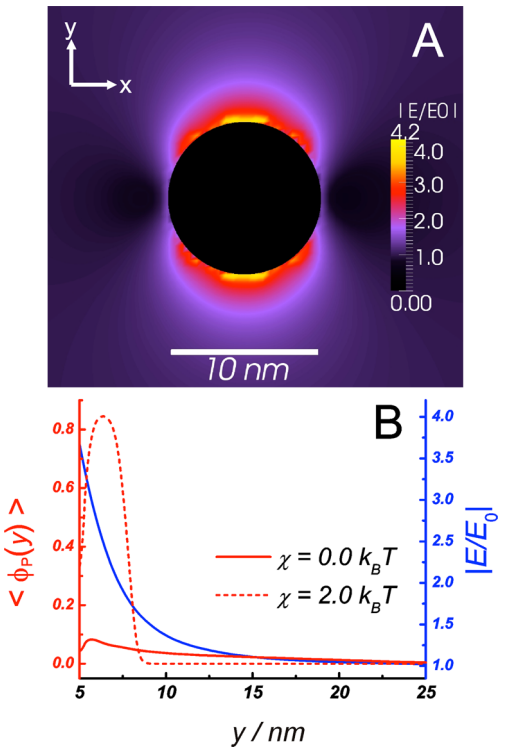

Figure 5. (A) Electric field contour plot for a nanoparticle of R = 5 nm, N = 150, σ = 0.25 chains·nm^{-2}, and χ = 0 k_BT. The propagation and polarization axes are x and y, respectively. (B) Electric field for the nanoparticle in A (right axis, blue curve) and polymer volume fraction profiles (left axis, red curve) for χ = 0 and 2.0 k_BT (same data as Figure 2). The origin of the y-axis is located at the center of the particle.

that $\Delta\lambda_{collapse}$ is always positive (*i.e.*, polymer collapse always red shifts the LSPR), which is in agreement with experimental findings.[3,16,18,19,22,23] This result is, in principle, not intuitive because decreasing film thickness and increasing polymer density (the two effects associated with polymer collapse) are expected to shift the LSPR in opposite directions (to higher and lower energies, respectively).[27] Our calculations show that the effect of increasing volume fraction always outweighs that of decreasing film thickness. This result can be understood by considering the strength of the electric near-field around the nanoparticle, shown in Figure 5A. In Figure 5B, we compare the field enhancement along the polarization axis (y) with the polymer density in the swollen and the collapsed states. This figure shows that the electric field decays exponentially with distance from the nanoparticle surface.[28,29] The region close to the surface is where the electric field enhancement is maximum and changes in the volume fraction occur mainly upon collapse. The LSPR is, therefore, more sensitive to the increase in polymer density close to the NP surface than to its decrease far from the surface. In the Supporting Information, we present an approximate model based on the spatial decay of the near-field, which predicts that polymer collapse always produces a red shift of the LSPR, in agreement with our calculations.

Another important result shown in Figure 4A is that the LSPR shift (2−5 nm for large N) is of the same order of magnitude as that experimentally observed for Au@PNIPAM (5−10 nm[3,16,18,19,23]). We will not attempt here a quantitative comparison between our theoretical predictions and the experiments because experimental values for N and σ are unknown. Furthermore, our model is not intended to reproduce the behavior of PNIPAM and the physical properties of the shells used in the experiments (these shells have a 5−10% cross-linking density and are thicker than the ones described here).

Shift of the LSPR Peak upon Polymer Collapse Depends Nonmonotonically on Grafting Density. Figure 4A shows that $\Delta\lambda_{collapse}$ increases monotonically with N, the chain length. This result is in qualitative agreement with the experimental results of Contreras−Caceres and coworkers,[18] who found an increase in the temperature sensitivity of the plasmon band of Au@PNIPAM with increasing shell thickness. Figure 4A also shows that $\Delta\lambda_{collapse}$ depends nonmonotonically on the grafting density. This important observation shows that increasing the amount of polymer in the system does not always maximize the LSPR sensitivity to polymer collapse.

In order to understand the nonmonotonic variation of $\Delta\lambda_{collapse}$ with grafting density, we need to study how the polymer collapse affects film thickness and inner volume fraction. The changes in these two variables are connected, so it is enough to analyze one of them. In the previous section, we have shown that λ^{LSPR} is more sensitive to changes in the internal volume fraction of the polymer than to changes in

thickness, so we calculate the average volume fraction for the film (ϕ^{mean}, see eq 8 in Methods) and its change upon film collapse (eq 2)

$$\Delta\phi^{mean}_{collapse} = \phi^{mean}(\chi = 2k_BT) - \phi^{mean}(\chi = 0k_BT) \quad (2)$$

Figure 4B shows that $\Delta\phi^{mean}_{collapse}$ is a nonmonotonic function of σ, in line with the trend observed for $\Delta\lambda_{collapse}$. The reason for the nonmonotonic dependence of $\Delta\phi^{mean}_{collapse}$ on grafting density is the following: for low grafting densities, there is not enough polymer in the system to substantially increase the polymer density around the particle upon collapse. In the limit of high grafting densities, the polymer volume fraction in the swollen state is already high and, thus, increases marginally upon collapse. The maximum in $\Delta\lambda_{collapse}$ and $\Delta\phi^{mean}_{collapse}$ is therefore achieved at intermediate values of σ.

Sensitivity of the LSPR Peak to Polymer Collapse Depends on the Position of the Plasmon Peak. Miller and Lazarides studied the sensitivity of the LSPR peak position for Au nanoparticles and nanoshells of different size and shape with variation of the refractive index for an infinite dielectric environment.[30] A main conclusion of that work was that the sensitivity of LSPR to the dielectric environment, also known as the refractive index sensitivity or RIS, increases linearly with the position of the LSPR. A similar behavior is expected for $\Delta\lambda_{collapse}$; to study this, we have calculated the optical properties of polymer-coated hollow Au NPs[6] for a fixed radius of the inorganic component (R = 30 nm) and different thicknesses of the Au shell (d_{Au}, see scheme in the inset of Figure 6A). In the calculations of Figure 6, the properties of the polymer layer do not depend on the thickness of the Au shell (because we keep the total radius of the inorganic component constant); therefore, this calculation isolates the effect of the position of the λ^{LSPR} on the sensitivity to collapse ($\Delta\lambda_{collapse}$).

Figure 6A shows that, as the thickness of the Au layer decreases, the LSPR band in the swollen state (λ^{LSPR} (χ = 0 k_BT)) shifts to lower energies. Figure 6B shows that $\Delta\lambda_{collapse}$ increases linearly with the position of the LSPR.[30,31] In other words, stimuli-modulated plasmon properties in Au@polymer systems can be enhanced by using Au NPs with the LSPR in the red/infrared region of the spectra. We note, however, that the polymer layer will behave differently for particles of different shape or size, and that this effect also impacts the LSPR. As we discuss next, in Au@polymer systems with cores of different sizes, there is a complex balance between the effects of polymer reorganization and the plasmon properties of the core.

Shift of the LSPR Peak upon Polymer Collapse Depends Nonmonotonically on Particle Radius. We turn our attention to the effect of particle size on $\Delta\lambda_{collapse}$ (for solid Au NPs). Figure 7A shows that $\Delta\lambda_{collapse}$ displays a broad

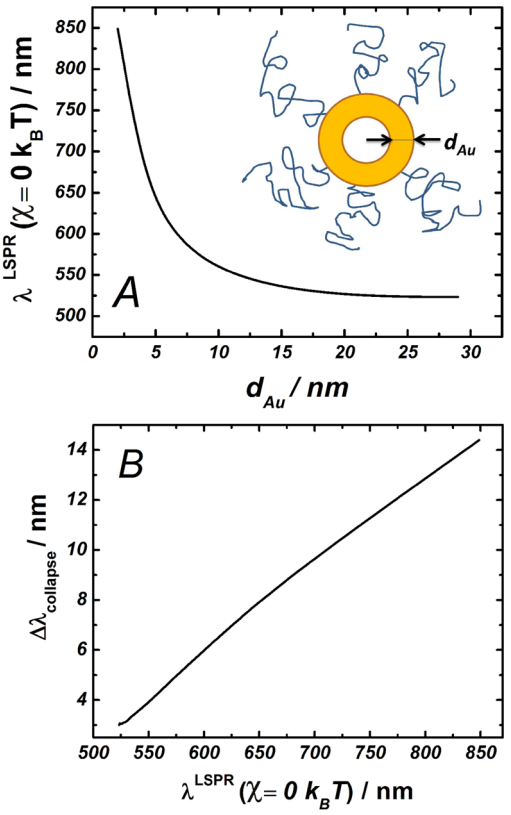

Figure 6. (A) Position of the LSPR band for polymer-coated Au hollow shell (σ = 0.5 chains·cm^{-2}, N = 150, R = 30 nm) as a function of the thickness of the gold layer for the swollen state (χ = 0 k_BT). (B) Change in the position of the LSPR upon polymer collapse as a function of the position of LSPR in the swollen state.

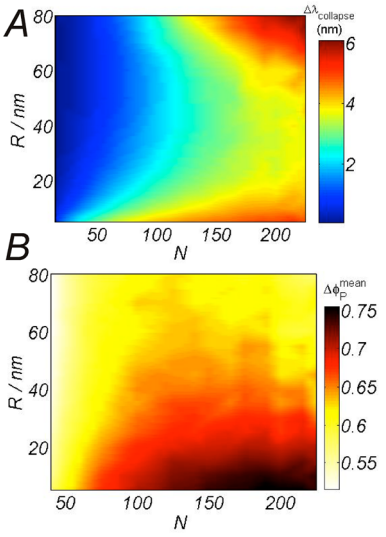

Figure 7. Change in the position of the LSPR band ($\Delta\lambda_{collapse}$, see eq 1, panel A) and the average polymer volume fraction of the film ($\Delta\phi^{mean}_{collapse}$, see eq 2, panel B) upon film collapse, as a function of chain length (N) and radius of the Au NP core (R). The polymer surface coverage is σ = 0.5 chains·nm^{-2}.

minimum with R for $R \sim 20-60$ nm. The reason that $\Delta\lambda_{collapse}$ increases for $R > 60$ nm is that the LSPR peak

of Au NPs begins to shift dramatically to the red due to coupling of the plasmon to far-field radiation, which partially quenches the resonance and broadens the LSPR (see, for example, ref 28). As we have shown in the previous section, shifting the LSPR to the red increases $\Delta\lambda_{collapse}$.

The decrease in $\Delta\lambda_{collapse}$ with R for R < 20 nm originates from the properties of the soft material shell. Figure 7B shows that the change in the average polymer volume fraction upon collapse, $\Delta\phi^{mean}_{collapse}$, defined in eq 2, is larger for smaller particles. This effect causes the increase of $\Delta\lambda_{collapse}$ for decreasing R. The reason why $\Delta\phi^{mean}_{collapse}$ is larger for smaller particles is that polymer chains in the swollen state are less packed on highly curved surfaces[12] and, therefore, their density decreases with decreasing core size (see Supporting Information Figure S1). On the other hand, the density of the collapsed state is rather constant. Consequently, the change in polymer density upon collapse is larger for smaller particles.

The complex nonmonotonic behavior of $\Delta\lambda_{collapse}$ with σ and R (Figures 4A and 7A) is a direct consequence of the interplay between the conformational properties of the polymer shell and the optical properties of the plasmonic core. This complexity highlights the importance of explicitly considering the physical properties of both the inorganic and the soft material components.

Breaking Spherical Symmetry and the Effect of Domain Formation on the LSPR Shift. In sections 2−6, we have analyzed films with a homogeneous thickness at each point on the NP surface (these films present inhomogeneities only in the radial coordinate). Polymers end-grafted to planar or curved surfaces in poor solvent can, however, microphase segregate[7,24,32−34] to form aggregates and thus break the original planar or spherical symmetry of the system. Microphase segregation occurs because grafting of the end group prevents the polymer from diffusing on the surface and thus frustrates macrophase separation in poor solvents.[24,35] In the microphase-segregated state, multiple local minima of the free energy, which correspond to aggregates of different size and shape, are possible. Figure 8 shows polymer volume fraction color maps for a Au@polymer NP in a good solvent (χ = 0 k_BT, Figure 8A) and a poor solvent (χ = 2 k_BT, Figure 8B,C). These calculations were performed using a cylindrical symmetry and allowing inhomogeneities in the radial (r) and longitudinal (z) coordinates. The morphologies in Figure 8B ("eccentric film", *i.e.*, a film slightly thicker on one side of the particle than on the other) and 8C ("janus film") were obtained for the same system parameters. In other words, these two morphologies correspond to two local minima of the free energy landscape. The janus morphology is more stable than the eccentric one by 4.5 k_BT per polymer chain.

Figure 9 shows the value of $\lambda^{LSPR}(\chi)-\lambda^{LSPR}(\chi=0)$ as a function of χ calculated for the morphologies in

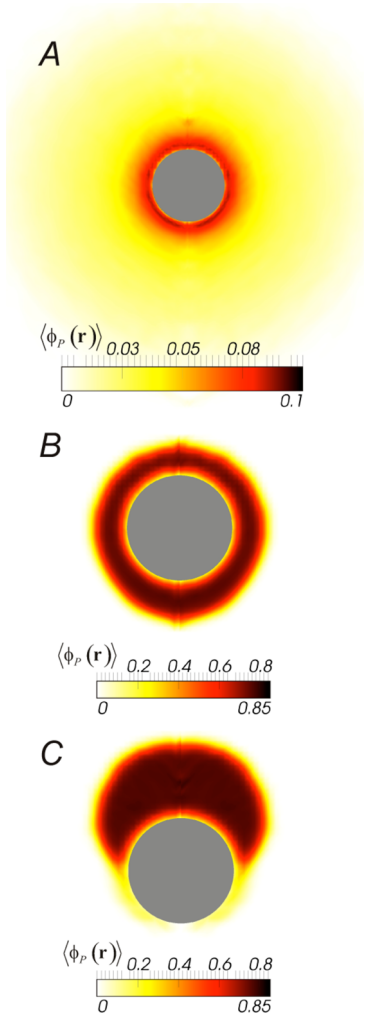

Figure 8. Color maps showing the polymer volume fraction in a plane containing the center of the particle. The calculations were performed assuming cylindrical symmetry and a homogeneous system in the angular coordinate (*i.e.*, only inhomogeneities in r and z). The figures correspond to a Au core of R = 5 nm coated with an end-grafted polymer layer of σ = 0.25 chains·nm^{-2}, N = 150, and χ = 0 k_BT (A) or 2.0 k_BT (B,C). The systems shown in B (eccentric) and C (janus) correspond to two minima of the free energy for the same calculation conditions.

Figure 8A−C. The figure shows that $\Delta\lambda_{collapse}$ is always positive and smaller for the janus film than for the eccentric one. Note that the janus and eccentric curves converge for χ = 1.2 k_BT because at this point the homogeneous film becomes thermodynamically stable and microphase segregation disappears.[35] We also plot the $\lambda^{LSPR}(\chi)-\lambda^{LSPR}(\chi=0)$ curve calculated for the spherical symmetrical system described in Figure 2, which almost overlaps that of the eccentric 2D calculation. The results in Figure 9 suggest that (i) homogeneously coating the NP maximizes the sensitivity of the LSPR to polymer collapse, and (ii) the results predicted in sections 2−6 may underestimate $\Delta\lambda_{collapse}$ when microphase segregation occurs. In the case of neutral polymers, microphase segregation is favored for relatively low grafting densities.[7]

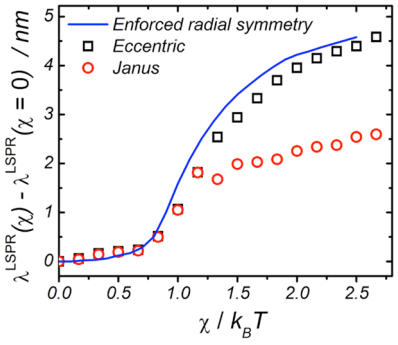

Figure 9. Change in the position of the LSPR when increasing the effective segment−segment interaction strength from $\chi = 0$ k_BT to χ for the systems shown in Figure 8 (calculation in cylindrical geometry with inhomogeneities in *r* and *z*, spontaneous symmetry breaking allowed) and Figure 2 (calculation in spherical geometry with inhomogeneities in *r*, enforced radial symmetry).

CONCLUSIONS

We have presented a new approach to model the optical properties of hybrid soft plasmonic materials and applied it to analyze the behavior of the LSPR in the Au@polymer system. Our results are in qualitative agreement with available experimental evidence, namely, (i) polymer collapse always produces a red shift of the LSPR,[3,16−19,23] (ii) the magnitude of the shift for spherical NPs is of the order of a few nanometers (<10 nm),[3,16−19,23] (iii) the sensitivity of Au@polymer systems to collapse increases with film thickness (*i.e.*, larger *N*),[18] and (iv) Au@polymer systems exhibiting LSPR at lower energies present larger shifts of the plasmon peak upon polymer collapse[18,19] (although, in this case, the effect of complex particle shapes on polymer morphology remains largely unexplored and may play a role). Our theory also predicts that the magnitude of the collapse-induced shift of the LSPR is a complicated function of the polymer grafting density, core radius, and formation of polymer aggregates. In these cases, systematic experiments are needed to corroborate these predictions and maximize the sensitivity of the LSPR to the chemical/physical stimuli.

We have studied a model polymer responsive to changes in the quality of the solvent (given by the parameter χ). We note that our theory can be straightforwardly extended to study Au@polymer NPs responsive to environmental changes of temperature,[36] pH,[24,37] redox potential,[38,39] or concentration of biological ligands.[40] Moreover, the molecular theory approach used here can be extended to other polymer topologies used in Au@polymer composites beyond the end-grafted homopolymer studied here, such as pH-sensitive grafted layers,[12] pH- and redox-responsive electrostatically adsorbed polymer layers,[38,39] gels,[41] or block copolymers.[42,43] It is also possible to use our methodology to study systems where changes in size or shape of the soft matter component modulate the distance between plasmonic nanoparticles and thus the plasmon coupling between them. This type of calculation will allow decoupling of the contributions of interparticle plasmon coupling and changes of refractive index to the shift of the plasmon resonance in, for example, the optical response of nanorod-coated PNIPAM microgels.[2]

The molecular theory used in this work is well-suited to study the structure of polymer systems because it allows systematic calculations at a fraction of the computational cost required by typical computer simulations, and it can be easily extended to model the effects of pH, redox potential, or chemical equilibria. The general concept behind our approach is not, however, limited to the molecular theory. For example, if a more detailed chemical model of the polymer is required, atomistic molecular dynamic simulations can be used to determine the local density and dielectric function around the nanoparticle, which are required in the electrodynamics calculations. Understanding hybrid materials requires hybrid theoretical models and we believe that, as the complexity of hybrid soft/plasmonic materials increases, our approach will be useful to provide design rules and fundamental understanding.

METHODS

We model the end-grafted polymer layer using a molecular theory that explicitly considers the shape, size, conformation, and molecular interactions of all of the species in the system.[24,37] For a detailed description of the analytical derivation and numerical implementation of the molecular theory, the reader is referred to ref 37 (one-dimensional inhomogeneities in spherical coordinates) and the article and Supporting Information of ref 7 (two-dimensional inhomogeneities in cylindrical coordinates). The predictions of the theory have been found to properly describe structural, thermodynamic, and functional properties of end-tethered neutral and charged polymers as compared with full-scale coarse-grained computer simulations[44,45] and with experimental observations.[8,38,46−48]

Briefly, we formulate the theory by writing down the free energy of the system as a functional of the distribution of the different molecular species and the probabilities of the different polymer conformations. More specifically, we write

$$\beta W = \int \rho_s(\mathbf{r})[\ln(\rho_s(\mathbf{r})v_s) - 1]d\mathbf{r} + \sigma \int_A \sum_\alpha P_p(\mathbf{r}(\mathbf{s}),\alpha)\ln(P_p(\mathbf{r}(\mathbf{s}),\alpha))d\mathbf{s} - \frac{\beta\chi}{2}\iint\left(\frac{a}{|\mathbf{r}-\mathbf{r}'|}\right)^6 f(|\mathbf{r}-\mathbf{r}'|)\langle n_p(\mathbf{r})\rangle\langle n_p(\mathbf{r}')\rangle d\mathbf{r}d\mathbf{r}' \quad (3)$$

where $\beta = 1/k_BT$. The first term in eq 3 corresponds to the translational entropy of the solvent, where $\rho_s(\mathbf{r})$ and v_s are the number density and volume of the solvent molecules (v_s = 0.03 nm^3), respectively. The second term is the conformational entropy of the polymer chains, where $P_p(\mathbf{r}(\mathbf{s}),\alpha)$ is the probability of having the polymer chain grafted at $\mathbf{r}(\mathbf{s})$ in conformation α, where $\mathbf{s}$ is a parametrization of the surface where the chains are

grafted and d**s** is the area element. The summation in this term runs over all possible chain conformations (although in practice we use a very large representative set). These conformations are generated in free space for the given values of N and R. The last term represents the van der Waals (vdW) effective attractive interactions between polymer segments. Here a is the segment length (a = 0.5 nm), χ is the strength of the effective segment−segment interactions, $f(|\mathbf{r}-\mathbf{r}'|)$ is a cutoff function that is 1 for $a < |\mathbf{r}-\mathbf{r}'| < 2.5\,\delta$ (with δ = 0.5 nm) or 0 otherwise and $\langle n_p(\mathbf{r})\rangle$ is the ensemble average number density of polymer segments at **r**:

$$\langle n_p(\mathbf{r})\rangle = \sigma \int \sum_{\alpha} P_p(\mathbf{r}'(\mathbf{s}'), \alpha) n(\mathbf{r}'(\mathbf{s}'), \alpha, \mathbf{r}) d\mathbf{s}' \quad (4)$$

where $n(\mathbf{r}'(\mathbf{s}'),\alpha,\mathbf{r})d\mathbf{r}$ is the number of the segments that a chain in conformation α grafted at $\mathbf{r}'(\mathbf{s}')$ has in the volume element between **r** and **r** + d**r** and the integral runs over the area where polymers are grafted.

The intermolecular repulsions are modeled as excluded volume interactions, and they are incorporated on a mean-field level through the packing (incompressibility) constraints

$$\langle n_p(\mathbf{r})\rangle v_p + \rho_s(\mathbf{r}) v_s = 1 \quad (5)$$

where v_p is the polymer segment volume (v_P = 0.095 nm^3).

The parameters relevant for the system under study are χ, σ, N, and R. The parameter χ controls the strength of the segment−segment attractions; that is, it is a multiplicative factor in the vdW interaction energy term in eq 3. The surface grafting density, σ, and the nanoparticle radius, R, determine the total number of chains in the system and appear in the theory in eqs 3 and 4 (R is implicit in the parametrization of the nanoparticle surface given by **s**). Finally, the number of segments per chain, N, enters the theory in the generation of the set of chain conformations (R also affects this set since the generated conformations avoid the nanoparticle). The specific segment distribution of each generated conformation determines the function $n(\mathbf{r}'(\mathbf{s}'),\alpha,\mathbf{r})$ in eq 4.

In order to solve the theory, we perform a functional minimization of eq 3 with respect with the density of the mobile species and the probability of each polymer conformation in order to obtain a set of coupled integro-differential equations. We discretize these equations into a system of nonlinear equations that we solve using numerical methods.

As an output from the theory, we obtain the functional forms for the density of mobile species and the probability of each polymer conformation in the equilibrium state, including the **r**-dependent polymer volume fraction:

$$\langle \phi_p(\mathbf{r})\rangle = \langle \rho_p(\mathbf{r})\rangle v_p \quad (6)$$

We calculate the **r**-dependent refractive index of the soft shell, $n(\mathbf{r})$, from $\langle \phi_p(\mathbf{r})\rangle$ using the Lorentz−Lorenz mixing rule for binary mixtures:[49,50]

$$\frac{n(\mathbf{r})^2 - 1}{n(\mathbf{r})^2 + 2} = (1 - \langle \phi_p(\mathbf{r})\rangle)\frac{n_s^2 - 1}{n_s^2 + 2} + \langle \phi_p(\mathbf{r})\rangle \frac{n_p^2 - 1}{n_p^2 + 2} \quad (7)$$

where n_s and n_p are the refractive indexes of the solvent (water, n_s = 1.33) and the polymer (n_p = 1.52, corresponding to the refractive index of PNIPAM and PVP[51−53]), respectively. The mixing rule given by eq 7, one of the most commonly used mixing rules to calculate the refractive index of mixtures, is based on the Clausius−Mossotti (CM) equation, which relates the dielectric constant and the molecular polarizabilities.[54] The quantitative results of our calculations are not affected by the choice of mixing expression; see Figure S2 in the Supporting Information. We finally calculate the optical properties of the polymer-coated nanoparticles by solving Maxwell's equations. We adopt different strategies to solve the molecular theory and calculate the optical properties of the Au@polymer colloids depending on the symmetry of the system. For the calculations in Figures 2−7, we assumed a spherical symmetry with inhomogeneities in the radial coordinate (the distance from the center of the sphere).[37] This strategy reduces the number of relevant dimensions to one, allowing very fast calculations. As an output from the theory, we obtain the radial-dependent refractive index of the system, $n(r)$, which we use to determine the optical properties. In practice, we discretize $n(r)$ into layers of thickness δ = 0.5 nm (which is the same discretization step used for the molecular theory) and use the open-source multilayer Mie theory code *scattnlay*[55] (the multilayer Mie theory is an analytical solution to the problem of calculating the optical properties of a spherical object with an inhomogeneous radial refractive index profile). We use the dielectric function of Johnson and Christy[56] for the Au core (for simplicity, we neglect the corrections to the gold dielectric function due to scattering of the electrons on the boundaries of the metal particle[57]). The extinction coefficients Q_{ext} reported in Figure 2 are calculated as $C_{ext}/(R^2\pi)$, where C_{ext} is the extinction cross section and R is the radius of the gold core.

For the calculations in Figures 8 and 9, we allow the system to spontaneously break the spherical symmetry upon collapse[7] by performing calculations within a cylindrical geometry that assumes inhomogeneities in the r and z coordinates.[7,9] The resulting nonlocal refractive index, $n(r,z)$, was then mapped into a Cartesian tridimensional grid (which completely contained the hybrid system and had a spacing of δ = 0.5 nm in the x, y, and z coordinates), and the optical properties were calculated with the discrete dipole approximation approach, as implemented in the open-source code *DDSCAT*.[58] The near-field in Figure 5 was also calculated with *DDSCAT*.

For spherical nanoparticles, it could be possible to use an effective medium theory (EMT) where the radially dependent refractive index is replaced by an effective refractive index estimated from the polymer volume fraction profile. However, for structures with a high degree of anisotropy, or where the electric field strength varies dramatically between resonances (for example, the longitudinal and transverse resonances of a nanorod), the effective refractive index in the EMT would need to be determined for each resonance, and therefore, the multilayer Mie theory or the DDA approaches to solve Maxwell's equations used in this work are more general than an EMT. Additionally, effective medium theories conceal the details of the electric field profile in the polymer, which is useful for the study of sensing devices.

We define mean quantities in the film from the theory as weighted averages, where the weighting factor is $\langle \phi_p(\mathbf{r})\rangle$ since this variable determines how much of the local value contributes to the value averaged over the film. In the specific case of the polymer volume fraction, the average value (used in eq 2) is

$$\phi^{mean} = \frac{\int \langle \phi_p(\mathbf{r})\rangle \langle \phi_p(\mathbf{r})\rangle d\mathbf{r}}{\int \langle \phi_p(\mathbf{r})\rangle d\mathbf{r}} \quad (8)$$

Conflict of Interest: The authors declare no competing financial interest.

Acknowledgment. This material is based upon work supported as part of the NERC (Non-Equilibrium Research Center), an Energy Frontier Research Center funded by the U.S. Department of Energy, Office of Science, Office of Basic Energy Sciences under Award Number DE-SC0000989. This research was supported in part through the computational resources and staff contributions provided by the Quest high performance computing facility at Northwestern University which is jointly supported by the Office of the Provost, the Office for Research, and Northwestern University Information Technology.

Supporting Information Available: Simple model based on the exponential decay of the electric field, polymer volume fraction in the swollen and collapsed states as a function of R and N, calculations for different refractive index mixing rules. This material is available free of charge *via* the Internet at http://pubs.acs.org.

REFERENCES AND NOTES

1. Stuart, M. A. C.; Huck, W. T. S.; Genzer, J.; Mueller, M.; Ober, C.; Stamm, M.; Sukhorukov, G. B.; Szleifer, I.; Tsukruk, V. V.; Urban, M.; *et al.* Emerging Applications of Stimuli-Responsive Polymer Materials. *Nat. Mater.* **2010**, *9*, 101–113.

2. Karg, M.; Pastoriza-Santos, I.; Perez-Juste, J.; Hellweg, T.; Liz-Marzan, L. M. Nanorod-Coated Pnipam Microgels: Thermoresponsive Optical Properties. *Small* **2007**, *3*, 1222–1229.
3. Alvarez-Puebla, R. A.; Contreras-Caceres, R.; Pastoriza-Santos, I.; Perez-Juste, J.; Liz-Marzan, L. M. Au@PNIPAM Colloids as Molecular Traps for Surface-Enhanced, Spectroscopic, Ultra-sensitive Analysis. *Angew. Chem., Int. Ed.* **2009**, *48*, 138–143.
4. Tokarev, I.; Minko, S. Tunable Plasmonic Nanostructures from Noble Metal Nanoparticles and Stimuli-Responsive Polymers. *Soft Matter* **2012**, *8*, 5980–5987.
5. Wu, S.; Dzubiella, J.; Kaiser, J.; Drechsler, M.; Guo, X.; Ballauff, M.; Lu, Y. Thermosensitive Au-PNIPA Yolk-Shell Nanoparticles with Tunable Selectivity for Catalysis. *Angew. Chem., Int. Ed.* **2012**, *51*, 2229–2233.
6. Zhu, Z.; Senses, E.; Akcora, P.; Sukhishvili, S. A. Programmable Light-Controlled Shape Changes in Layered Polymer Nanocomposites. *ACS Nano* **2012**, *6*, 3152–3162.
7. Peleg, O.; Tagliazucchi, M.; Kroeger, M.; Rabin, Y.; Szleifer, I. Morphology Control of Hairy Nanopores. *ACS Nano* **2011**, *5*, 4737–4747.
8. Tagliazucchi, M.; Azzaroni, O.; Szleifer, I. Responsive Polymers End-Tethered in Solid-State Nanochannels: When Nanoconfinement Really Matters. *J. Am. Chem. Soc.* **2010**, *132*, 12404–12411.
9. Tagliazucchi, M.; Rabin, Y.; Szleifer, I. Ion Transport and Molecular Organization Are Coupled in Polyelectrolyte-Modified Nanopores. *J. Am. Chem. Soc.* **2011**, *133*, 17753–17763.
10. Calvo, A.; Yameen, B.; Williams, F. J.; Azzaroni, O.; Soler-Illia, G. Facile Molecular Design of Hybrid Functional Assemblies with Controllable Transport Properties: Mesoporous Films Meet Polyelectrolyte Brushes. *Chem. Commun.* **2009**, 2553–2555.
11. Calvo, A.; Yameen, B.; Williams, F. J.; Soler-Illia, G. J. A. A.; Azzaroni, O. Mesoporous Films and Polymer Brushes Helping Each Other To Modulate Ionic Transport in Nanoconfined Environments. An Interesting Example of Synergism in Functional Hybrid Assemblies. *J. Am. Chem. Soc.* **2009**, *131*, 10866–10868.
12. Tagliazucchi, M.; Szleifer, I. Stimuli-Responsive Polymers Grafted to Nanopores and Other Nano-Curved Surfaces: Structure, Chemical Equilibrium and Transport. *Soft Matter* **2012**, *8*, 3292–3305.
13. Frickel, N.; Messing, R.; Schmidt, A. M. Magneto-Mechanical Coupling in $CoFe_2O_4$-Linked Paam Ferrohydrogels. *J. Mater. Chem.* **2011**, *21*, 8466–8474.
14. Kaiser, A.; Winkler, M.; Krause, S.; Finkelmann, H.; Schmidt, A. M. Magnetoactive Liquid Crystal Elastomer Nanocomposites. *J. Mater. Chem.* **2009**, *19*, 538–543.
15. Chapman, R.; Mulvaney, P. Electro-Optical Shifts in Silver Nanoparticle Films. *Chem. Phys. Lett.* **2001**, *349*, 358–362.
16. Contreras-Caceres, R.; Sanchez-Iglesias, A.; Karg, M.; Pastoriza-Santos, I.; Perez-Juste, J.; Pacifico, J.; Hellweg, T.; Fernandez-Barbero, A.; Liz-Marzan, L. M. Encapsulation and Growth of Gold Nanoparticles in Thermoresponsive Microgels. *Adv. Mater.* **2008**, *20*, 1666–1670.
17. Li, D.; He, Q.; Yang, Y.; Mohwald, H.; Li, J. Two-Stage pH Response of Poly(4-vinylpyridine) Grafted Gold Nanoparticles. *Macromolecules* **2008**, *41*, 7254–7256.
18. Contreras-Caceres, R.; Pacifico, J.; Pastoriza-Santos, I.; Perez-Juste, J.; Fernandez-Barbero, A.; Liz-Marzan, L. M. Au@PNIPAM Thermosensitive Nanostructures: Control over Shell Cross-Linking, Overall Dimensions, and Core Growth. *Adv. Funct. Mater.* **2009**, *19*, 3070–3076.
19. Fernandez-Lopez, C.; Perez-Balado, C.; Perez-Juste, J.; Pastoriza-Santos, I.; de Lera, A. R.; Liz-Marzan, L. M. A General LbL Strategy for the Growth of PNIPAM Microgels on Au Nanoparticles with Arbitrary Shapes. *Soft Matter* **2012**, *8*, 4165–4170.
20. Volden, S.; Kjoniksen, A.-L.; Zhu, K.; Genzer, J.; Nystrom, B.; Glomm, W. R. Temperature-Dependent Optical Properties of Gold Nanoparticles Coated with a Charged Diblock Copolymer and an Uncharged Triblock Copolymer. *ACS Nano* **2010**, *4*, 1187–1201.
21. Guo, L.; Nie, J.; Du, B.; Peng, Z.; Tesche, B.; Kleinermanns, K. Thermoresponsive Polymer-Stabilized Silver Nanoparticles. *J. Colloid Interface Sci.* **2008**, *319*, 175–181.
22. Jonas, A. M.; Hu, Z. J.; Glinel, K.; Huck, W. T. S. Effect of Nanoconfinement on the Collapse Transition of Responsive Polymer Brushes. *Nano Lett.* **2008**, *8*, 3819–3824.
23. Nuopponen, M.; Tenhu, H. Gold Nanoparticles Protected with pH and Temperature-Sensitive Diblock Copolymers. *Langmuir* **2007**, *23*, 5352–5357.
24. Tagliazucchi, M.; Olvera de la Cruz, M.; Szleifer, I. Self-Organization of Grafted Polyelectrolyte Layers *via* the Coupling of Chemical Equilibrium and Physical Interactions. *Proc. Natl. Acad. Sci. U.S.A.* **2010**, *107*, 5300–5305.
25. Netz, R. R.; Andelman, D. Neutral and Charged Polymers at Interfaces. *Phys. Rep.* **2003**, *380*, 1–95.
26. Alexander, S. Adsorption of Chain Molecules with a Polar Head—A Scaling Description. *J. Phys. (Paris)* **1977**, *38*, 983–987.
27. Malinsky, M. D.; Kelly, K. L.; Schatz, G. C.; Van Duyne, R. P. Chain Length Dependence and Sensing Capabilities of the Localized Surface Plasmon Resonance of Silver Nanoparticles Chemically Modified with Alkanethiol Self-Assembled Monolayers. *J. Am. Chem. Soc.* **2001**, *123*, 1471–1482.
28. Harris, N.; Blaber, M. G.; Schatz, G. C. Optical Properties of Metal Nanoparticles. In *Enclopedia of Nanotechnology*, Bhushan, B., Ed.; Springer: Berlin, 2012; Vol. 481, pp 9751−9754.
29. Kelly, K. L.; Coronado, E.; Zhao, L. L.; Schatz, G. C. The Optical Properties of Metal Nanoparticles: The Influence of Size, Shape, and Dielectric Environment. *J. Phys. Chem. B* **2003**, *107*, 668–677.
30. Miller, M. M.; Lazarides, A. A. Sensitivity of Metal Nanoparticle Surface Plasmon Resonance to the Dielectric Environment. *J. Phys. Chem. B* **2005**, *109*, 21556–21565.
31. Averitt, R. D.; Sarkar, D.; Halas, N. J. Plasmon Resonance Shifts of Au-Coated Au_2s Nanoshells: Insight into Multicomponent Nanoparticle Growth. *Phys. Rev. Lett.* **1997**, *78*, 4217–4220.
32. Williams, D. R. M. Grafted Polymers in Bad Solvents - Octupus Surface Micelles. *J. Phys. II* **1993**, *3*, 1313–1318.
33. Pattanayek, S. K.; Pham, T. T.; Pereira, G. G. Morphological Structures Formed by Grafted Polymers in Poor Solvents. *J. Chem. Phys.* **2005**, *122*, 214908.
34. Sandberg, D. J.; Carrillo, J. M. Y.; Dobrynin, A. V. Molecular Dynamics Simulations of Polyelectrolyte Brushes: From Single Chains to Bundles of Chains. *Langmuir* **2007**, *23*, 12716–12728.
35. Gong, P.; Genzer, J.; Szleifer, I. Phase Behavior and Charge Regulation of Weak Polyelectrolyte Grafted Layers. *Phys. Rev. Lett.* **2007**, *98*, 018302.
36. Ren, C.-l.; Nap, R. J.; Szleifer, I. The Role of Hydrogen Bonding in Tethered Polymer Layers. *J. Phys. Chem. B* **2008**, *112*, 16238–16248.
37. Nap, R.; Gong, P.; Szleifer, I. Weak Polyelectrolytes Tethered to Surfaces: Effect of Geometry, Acid-Base Equilibrium and Electrical Permittivity. *J. Polym. Sci., Part B: Polym. Phys.* **2006**, *44*, 2638–2662.
38. Tagliazucchi, M.; Calvo, E. J.; Szleifer, I. Redox and Acid Base Coupling in Ultrathin Polyelectrolyte Films. *Langmuir* **2008**, *24*, 2869–2877.
39. Tagliazucchi, M.; Calvo, E. J.; Szleifer, I. Molecular Theory of Chemically Modified Electrodes by Redox Polyelectrolytes under Equilibrium Conditions: Comparison with Experiment. *J. Phys. Chem. C* **2008**, *112*, 458–471.
40. Longo, G.; Szleifer, I. Ligand-Receptor Interactions in Tethered Polymer Layers. *Langmuir* **2005**, *21*, 11342–11351.
41. Longo, G. S.; de la Cruz, M. O.; Szleifer, I. Molecular Theory of Weak Polyelectrolyte Thin Films. *Soft Matter* **2012**, *8*, 1344–1354.
42. Fang, F.; Szleifer, I. Controlled Release of Proteins from Polymer-Modified Surfaces. *Proc. Natl. Acad. Sci. U.S.A.* **2006**, *103*, 5769–5774.
43. Szleifer, I.; Carignano, M. A. Tethered Polymer Layers: Phase Transitions and Reduction of Protein Adsorption. *Macromol. Rapid Commun.* **2000**, *21*, 423–448.

44. Carignano, M. A.; Szleifer, I. Structural and Thermodynamic Properties of End-Grafted Polymers on Curved Surfaces. *J. Chem. Phys.* **1995**, *102*, 8662–8669.
45. Carignano, M. A.; Szleifer, I. On the Structure and Pressure of Tethered Polymer Layers in Good Solvent. *Macromolecules* **1995**, *28*, 3197–3204.
46. Gong, P.; Wu, T.; Genzer, J.; Szleifer, I. Behavior of Surface-Anchored Poly(acrylic acid) Brushes with Grafting Density Gradients on Solid Substrates: 2. Theory. *Macromolecules* **2007**, *40*, 8765–8773.
47. Carignano, M. A.; Szleifer, I. Pressure Isotherms, Phase-Transition, Instability, and Structure of Tethered Polymers in Good, Theta, and Poor Solvents. *J. Chem. Phys.* **1994**, *100*, 3210–3223.
48. Faure, M. C.; Bassereau, P.; Carignano, M. A.; Szleifer, I.; Gallot, Y.; Andelman, D. Monolayers of Diblock Copolymer at the Air−Water Interface: The Attractive Monomer-Surface Case. *Eur. Phys. J. B* **1998**, *3*, 365–375.
49. Heller, W. Remarks on Refractive Index Mixing Rules. *J. Phys. Chem.* **1965**, *69*, 1123–1129.
50. Tasic, A. Z.; Djordjevic, B. D.; Grozdanic, D. K.; Radojkovic, N. Use of Mixing Rules in Predicting Refractive Indexes and Specific Refractivities for Some Binary-Liquid Mixtures. *J. Chem. Eng. Data* **1992**, *37*, 310–313.
51. Erbe, A.; Tauer, K.; Sigel, R. Ellipsometric Light Scattering for the Characterization of Thin Layers on Dispersed Colloidal Particles. *Phys. Rev. E* **2006**, *73*, 031406.
52. Reufer, M.; Diaz-Leyva, P.; Lynch, I.; Scheffold, F. Temperature-Sensitive Poly(*N*-isopropyl-acrylamide) Microgel Particles: A Light Scattering Study. *Eur. Phys. J. E* **2009**, *28*, 165–171.
53. Senowa, R. J.; Sankhla, S.; Sharma, S. Refractometric Study of Polymers and Their Blends in Solution. *Indian J. Chem. A* **2007**, *46*, 1419–1422.
54. Aspnes, D. E. Optical-Properties of Thin-Films. *Thin Solid Films* **1982**, *89*, 249–262.
55. Pena, O.; Pal, U. Scattering of Electromagnetic Radiation by a Multilayered Sphere. *Comput. Phys. Commun.* **2009**, *180*, 2348–2354.
56. Johnson, P. B.; Christy, R. W. Optical Constants of Noble Metals. *Phys. Rev. B* **1972**, *6*, 4370–4379.
57. Scaffardi, L. B.; Tocho, J. O. Size Dependence of Refractive Index of Gold Nanoparticles. *Nanotechnology* **2006**, *17*, 1309–1315.
58. Draine, B. T.; Flatau, P. J. Discrete-Dipole Approximation for Scattering Calculations. *J. Opt. Soc. Am. A* **1994**, *11*, 1491–1499.